J Mater Sci (2017) 52:13868–13878

Electronic materials

$NaScMo_2O_8:RE^{3+}$ (RE = Tb, Eu, Tb/Eu, Yb/Er, Yb/Ho) phosphors: hydrothermal synthesis, energy transfer and multicolor tunable luminescence

Dingyi Shen[1], Bei Zhao[1], Shunrong Yang[1], Shanshan Hu[1], Jianfeng Tang[2], Xianju Zhou[3], and Jun Yang[1,*]

[1] School of Chemistry and Chemical Engineering, Southwest University, No. 2 Tiansheng Road, Beibei District, Chongqing 400715, People's Republic of China

[2] Faculty of Materials and Energy, Southwest University, Chongqing 400715, People's Republic of China

[3] School of Mathematics and Physics, Chongqing University of Posts and Telecommunications, Chongqing 400065, People's Republic of China

Received: 12 April 2017
Accepted: 14 July 2017
Published online: 11 September 2017

ABSTRACT

$NaScMo_2O_8:RE^{3+}$ (RE = Tb, Eu, Tb/Eu, Yb/Er, Yb/Ho) phosphors were successfully synthesized by surfactant-free hydrothermal method and post-calcination treatment. The energy transfer (ET) of $MoO_4^{2-} \rightarrow Tb^{3+} \rightarrow Eu^{3+}$ was proved by photoluminescence spectra and decay features. Multicolor emissions (green → yellow → red) were obtained by adjusting the ratio of Tb^{3+}/Eu^{3+} upon excitation into the MoO_4^{2-} at 292 nm. The ET of $Tb^{3+} \rightarrow Eu^{3+}$ was demonstrated to be a resonant type via a dipole–dipole mechanism, and the crystal distance (R_c) was calculated by the quenching concentration method. Under 980 nm excitation, the emission of $NaScMo_2O_8:RE^{3+}$ (RE = Yb/Er, Yb/Ho) showed strong green (Yb^{3+}/Er^{3+}: $^4S_{3/2}$, $^2H_{11/2} \rightarrow {}^4I_{15/2}$; Yb^{3+}/Ho^{3+}: $^5S_2 \rightarrow {}^5I_8$) luminescence, respectively. Moreover, the doping concentration of the Yb^{3+} has been optimized under a fixed concentration of Er^{3+} and Ho^{3+}, respectively. The $NaScMo_2O_8:RE^{3+}$ phosphors have potential applications for color displays and light-emitting devices due to a variety of luminous colors.

Introduction

Inorganic luminescent materials have more excellent property such as low photobleaching, longer luminescent lifetimes and narrow emission bands than organic fluorescent dyes and semiconductor quantum dots [1–4]. Among various materials reported, rare-earth (RE)-doped molybdates have attracted considerable attention and been a significant research topic not only for the basic scientific interest but also for their remarkable photoelectronic performances in fields such as negative thermal expansion materials, photocatalysis, phosphors,

Address correspondence to E-mail: jyang@swu.edu.cn

DOI 10.1007/s10853-017-1396-8

solid-state lasers and catalysis [5, 6]. As a fascinating group of molybdates, double alkaline rare-earth molybdates $ARE(MoO_4)_2$ (A = Na, K; RE = trivalent rare-earth cations) with tetragonal and monoclinic symmetries have been widely reported owing to their high chemical durability, large rare-earth ions admittance and large absorption cross sections for luminescent hosts [7–9]. Particularly, they have a relatively low lattice phonon energy which would be conducive to prevent concentration quenching effect and increase the possibility of radiative transitions. It is beneficial to a high quantum yield of down/up conversion (DC/UC) process. Therefore, great endeavors have been devoted to prepare tetragonal $NaRE(MoO_4)_2$ (RE = Y, Gd, La, Eu, Ce) nano-/microstructured host materials which share the scheelite-like ($CaMoO_4$) iso-structure [2, 7–11]. However, lanthanide ion-doped $NaRE(MoO_4)_2$ with monoclinic phase have rarely been reported in previous work and there is no systematic research about the luminescent properties of monoclinic $NaScMo_2O_8:RE^{3+}$ [12].

Rare-earth elements played an important role in modern lighting and display fields due to their special electronic structure and profuse energy levels ($4f^n5s^25p^6$, $0 \le n \le 14$) [13, 14]. Among various RE^{3+} ions, Eu^{3+} is an important activator for red emission because of its intrinsic characteristic transition ($^5D_0 \rightarrow {}^7F_2$ at around 615 nm) [15, 16], which has already started commercial applications as red phosphors for decades (like $Y_2O_3:Eu^{3+}$), but it has weak-line absorption of f–f transitions in the near-ultraviolet (NUV) region [17, 18]. It is very significant to improve the luminescence efficiency of Eu^{3+} and the ratio of red emission (610–620 nm, $^5D_0 \rightarrow {}^7F_2$) to orange emission (590–600 nm, $^5D_0 \rightarrow {}^7F_1$) in Eu^{3+}. The energy transfer (ET) from sensitizers to activators in a proper host is an effective way to solve the above problem [19, 20]. Tb^{3+} ion, as a good sensitizer for the Eu^{3+} ion, not only enhance the luminescence efficiency of Eu^{3+} ions but also broaden the absorption region in $NaY(MoO_4)_2$ [12], $Na_3Gd(PO_4)_2$ [21], $SrMg_2LaW_2O_{12}$ [22] and $CaYAlO_4$ [23] phosphors owing to introduction of more impurity energy levels in the host. Furthermore, the emission color of phosphors can be regulated by changing the ratio of Tb^{3+} to Eu^{3+} ions. The UC emission is anti-Stokes emission process which has been the focus of much research due to the merits of the high photochemical stability, large anti-Stokes shifts, partially filled 4f orbitals, the absence of autofluorescence of biotissues and sharp emission lines [24]. Therefore, they were applied to the fields of biotechnologies, three-dimensional displays, optical temperature sensors, solar cells and optical amplifiers [25–27]. The UC process can be divided into three broad classes: excited-state absorption (ESA), energy transfer (ET) and photon avalanche (PA) [24]. The efficient UC phosphors is usually doped with rare-earth ions which has a unique set of energy levels and generally exhibits a set of sharp emission peaks with distinguishable spectroscopic fingerprints [28]. Yb^{3+} ions have a much larger near-infrared (NIR) absorption cross section, which are often co-doped as excellent sensitizers along with Er^{3+} or Ho^{3+} to yield strong red or green UC emissions [29]. The ET between RE^{3+} ions via the nonradiative process would result in tunable multicolor emissions.

In this paper, $NaScMo_2O_8$ phosphors have been proven to be an excellent host matrix for the luminescence of RE^{3+} (RE = Tb, Eu, Tb/Eu, Yb/Er, Yb/Ho), which were successfully synthesized by surfactant-free hydrothermal method and subsequent calcination at 800 °C. The obtained phosphors exhibited good emission properties when activated with RE^{3+} (RE = Tb, Eu, Tb/Eu, Yb/Er, Yb/Ho). It was found that multicolor emissions (green → yellow → red) were acquired due to the effective ET of $MoO_4^{2-} \rightarrow Tb^{3+} \rightarrow Eu^{3+}$. Furthermore, the energy transfer from Tb^{3+} to Eu^{3+} was dominant by dipole–dipole interaction. The efficient ET from Yb^{3+} to Er^{3+} (Ho^{3+}) also took place in $NaScMo_2O_8$ host to get UC luminescence.

Experimental section

Synthesis

In a typical process, 1 mmol of $ScCl_3$, appropriate stoichiometric $RECl_3$ and 35 ml deionized water were added into a 100-ml beaker firstly. After vigorous agitation for 10 min, 6 mmol $Na_2MoO_4{\cdot}2H_2O$ was dissolved in the above solution with strong magnetic stirring; then, a white colloidal suspension was obtained. The pH value was subsequently adjusted to 7 by dropwise adding NaOH solution. Under strong stirring for 30 min, the suspension was transferred into a 50-ml Teflon-lined autoclave sealed in a stainless steel vessel and maintained at 180 °C for 24 h.

After natural cooling, the hydrothermal products were washed with distilled water and alcohol several times and then dried at 60 °C for 12 h. Finally, the final products were collected after further calcination at 800 °C for 2 h (Fig. S1 in Supporting Information).

Characterization

Powder X-ray diffraction (XRD) was performed on a Purkinje General Instrument MSALXD3 using Cu Kα radiation ($\lambda = 0.15406$ nm) with a scanning rate of 10° min^{-1} in the 2θ range from 10° to 60° at 20 mA and 36 kV. The morphologies and energy-dispersive spectrometry (EDS) spectra of the samples were observed by means of a field emission-scanning electron microscope (FESEM, XL30, Philips) operated at an accelerating voltage of 10 kV. The DC fluorescence spectra were obtained using a Hitachi F-7000 spectrophotometer equipped with a 150-W xenon lamp as the excitation source, and the lifetime decays were measured on FLSP920 fluorescence spectrophotometer and Shimidazu R9287 photomultiplier (200–900 nm) equipped with a liquid-nitrogen-cooled InGaAs (800–1700 nm) as detector. The UC luminescence spectra were measured using a 980-nm laser with MDL-N-980-8 W as the excitation source and detected using a LS 55 (PerkinElmer) from 400 to 750 nm. All the measurements were performed at room temperature.

Results and discussion

Phase and morphology

The XRD pattern of the sodium scandium molybdate precursor sample is shown in Fig. S2 (Supporting Information). Compared with all the standard XRD patterns in JCPDS cards, the precursor cannot be indexed to a certain compound because the product produced by the hydrothermal method probably contains some hydrous compounds from the solution medium [6]. Figure 1 displays the XRD patterns of $NaScMo_2O_8$ and $NaScMo_2O_8$:RE^{3+} (RE = Tb, Eu, Tb/Eu, Yb/Er, Yb/Ho) samples annealed at 800 °C as well as the JCPDS card (No. 32-1150) for $NaScMo_2O_8$, respectively. All the patterns match well with the pure monoclinic phase (JCPDS#32-1150), and no additional peaks or other phases can be found, revealing that the doped RE^{3+} (RE = Tb, Eu, Tb/Eu, Yb/Er, Yb/Ho) ions have been effectively dissolved in the $NaScMo_2O_8$ host matrix. Notably, when the Sc^{3+} was substituted by the RE^{3+} with bigger radius, the corresponding XRD peaks shift to lower angle direction due to the Vegard law [1]. The relative peak intensity of [001] for the samples doped with RE^{3+} is visibly enhanced, implying that the prismatic structures of the $NaScMo_2O_8$:RE^{3+} (RE = Tb, Eu, Tb/Eu, Yb/Er, Yb/Ho) samples grow preferentially along the [001] direction. The strong and sharp diffraction peaks indicate good crystallinity of the as-prepared samples, which is good for luminescence.

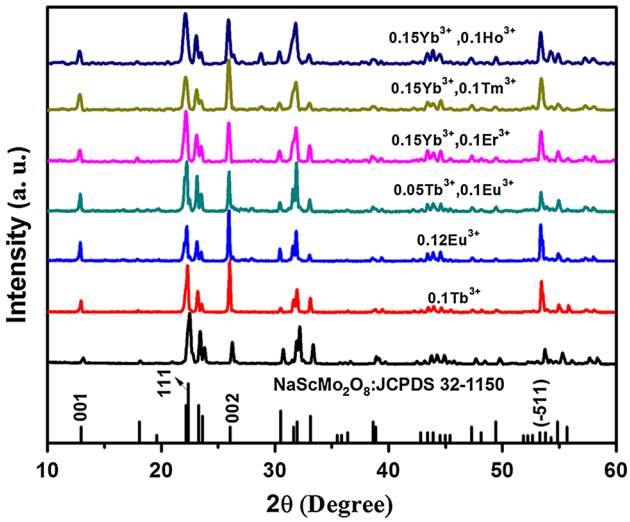

Figure 1 XRD patterns of the $NaScMo_2O_8$ and $NaScMo_2O_8$:RE^{3+} (RE = Tb, Eu, Tb/Eu, Yb/Er, Yb/Ho) samples. The standard data for $NaScMo_2O_8$ (JCPDS#32-1150) are also presented in the figure for comparison.

The morphology and chemical element of the sodium scandium molybdate precursor samples (Fig. 2a, c) and the corresponding $NaScMo_2O_8$ samples annealed at 800 °C for 2 h (Fig. 2b, d) were inspected by using SEM and EDS test, respectively. As shown in Fig. 2a, the SEM image of sodium scandium molybdate precursor sample consists of nonuniform rectangular sheets with size in micron level. After annealing at 800 °C for 2 h (Fig. 2b), the obtained $NaScMo_2O_8$ sample becomes irregular blocks with larger size due to the decomposition of the sodium scandium molybdate precursor sample during calcination process. This phenomenon can be proved by the EDS of the precursor in Fig. 2c, and the sodium scandium molybdate precursor may contain elements of C, Na, Sc, Mo and O (Table S1 in Supporting Information). The EDS in Fig. 2d suggests

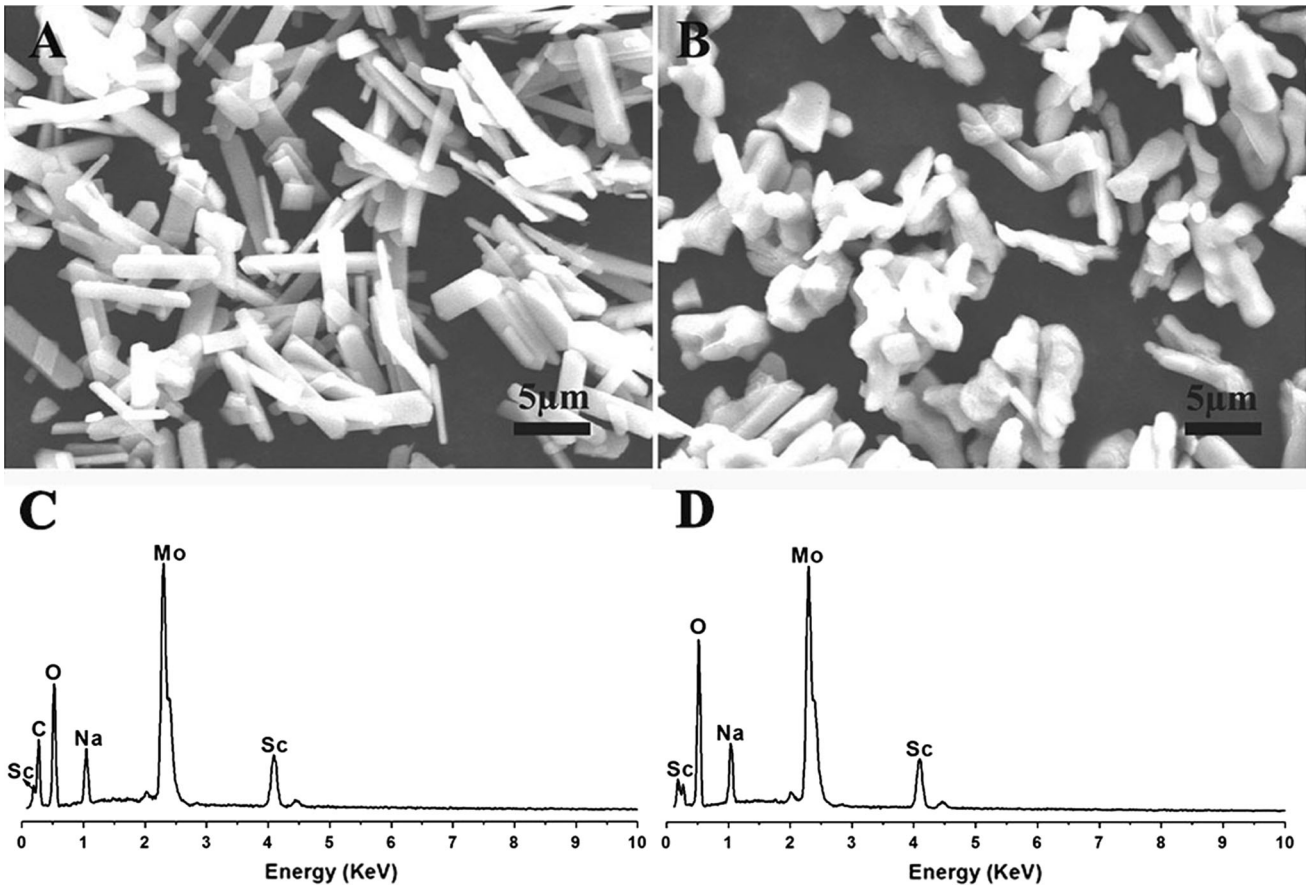

Figure 2 SEM images and EDS spectrum of the sodium scandium molybdate precursor sample (**a**, **c**) and the corresponding $NaScMo_2O_8$ sample annealed at 800 °C for 2 h (**b**, **d**).

that the calcined products are composed of Na, Sc, Mo and O elements with corresponding atomic ratio of 1.06:1.00:2.16:7.75, which is similar to the theoretical value (1:1:2:8) of the $NaScMo_2O_8$ crystals without considering the instrument error (Table S2 in Supporting Information).

Downconversion luminescence and energy transfer

The excitation and emission spectra of the $NaSc_{(1-x)}Mo_2O_8$:xTb^{3+} ($x = 0.01$–0.15) and $NaSc_{(1-x)}Mo_2O_8$:xEu^{3+} ($x = 0.01$–0.15) samples are shown in Fig. 3, respectively. The Tb^{3+} ions could be used as an activator for green-emitting materials owing to their $^5D_4 \rightarrow {}^7F_5$ transition, and the Eu^{3+} ions can be investigated as a red-emitting conversion phosphor due to their $^5D_0 \rightarrow {}^7F_2$ transition, respectively. As shown in Fig. 3a, upon excitation into the MoO_4^{2-} at 292 nm (Fig. S3 in Supporting Information), the emission spectrum (right) of Tb^{3+} consists of $^5D_4 \rightarrow {}^7F_6$ (492 nm) in the blue region, $^5D_4 \rightarrow {}^7F_5$ (549 nm, strongest peak) in the green region and $^5D_4 \rightarrow {}^7F_4$ (589 nm)/$^5D_4 \rightarrow {}^7F_3$ (625 nm) in the red region, which are much stronger than that of MoO_4^{2-} [6]. When monitored at 549 nm ($^5D_4 \rightarrow {}^7F_5$ of Tb^{3+}), there are two parts in the range of 200–500 nm, which are ascribed to the charge-transfer (C–T) transitions of Mo^{6+}–O^{2-} from 200 to 350 nm [9, 30–32] and the typical intraconfigurational f–f transitions of Tb^{3+} ions from 350 to 500 nm, respectively. Obviously, the characteristic excitation spectrum of Tb^{3+} becomes unapparent compared to that of MoO_4^{2-}. The above results illustrate that the energy transfer from MoO_4^{2-} to Tb^{3+} took place [33, 34]. Figure 3b displays the excitation spectrum (left) monitored at 618 nm ($^5D_0 \rightarrow {}^7F_2$ of Eu^{3+}), which consists of a broad and strong charge-transfer band of MoO_4^{2-} ranging from 200 to 350 nm with a maximum at around 292 nm and a series of typical f–f transitions of Eu^{3+} ions at 367 nm ($^7F_0 \rightarrow {}^5D_4$), 382 nm ($^7F_0 \rightarrow {}^5L_7$), 395 nm ($^7F_0 \rightarrow {}^5L_6$), 417 nm ($^7F_0 \rightarrow {}^5D_3$)

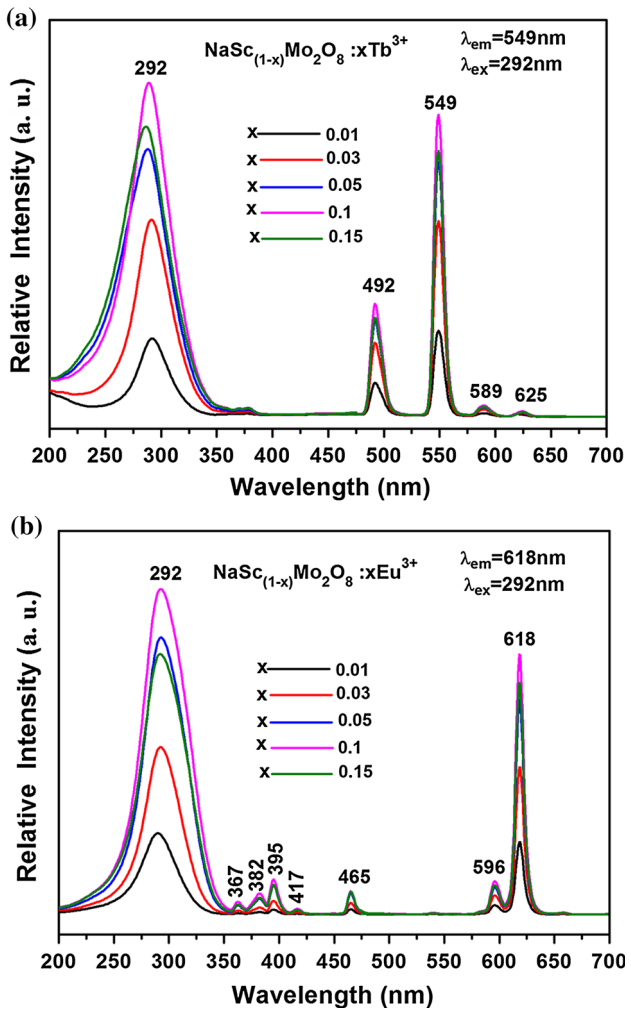

Figure 3 Excitation (*left*) and emission spectra (*right*) of the $NaSc_{(1-x)}Mo_2O_8$:xTb^{3+} ($x = 0.01$–0.15) samples (**a**) and the $NaSc_{(1-x)}Mo_2O_8$:xEu^{3+} ($x = 0.01$–0.15) samples (**b**).

and 465 nm ($^7F_0 \rightarrow {}^5D_2$), respectively. It is worth noting that the emission of Eu^{3+} under 292 nm excitation was mainly composed of the $^5D_0 \rightarrow {}^7F_1$ (596 nm) magnetic dipole transition and the $^5D_0 \rightarrow {}^7F_2$ (618 nm) electric dipole transition, respectively. The asymmetry ratio of I($^5D_0 \rightarrow {}^7F_2$)/I($^5D_0 \rightarrow {}^7F_1$) was equal to 7.8 which indicates that the Eu^{3+} ions have no inversion center in $NaScMo_2O_4$ host and the $NaScMo_2O_4$:Eu^{3+} product is beneficial to improve the color purity of the red phosphor. The energy transfer from MoO_4^{2-} to Eu^{3+} is similar to that from MoO_4^{2-} to Tb^{3+}. The doping concentration of the luminescent center has a significant impact on the performance of phosphors [35]. With increasing concentration of RE^{3+} ions, the resonance energy transfer is allowed because the distance of the luminescent centers becomes short enough to bring about concentration quenching of RE^{3+}. So, it is very important to find the optimum doping concentration. Obviously, the quenching concentration of Tb^{3+} or Eu^{3+} in $NaScMo_2O_8$ host both is 10% (Fig. 3), indicating that $NaScMo_2O_8$ is a good matrix for luminescent materials like $GdY(MoO_4)_3$:RE^{3+} (RE = Eu, Dy, Sm, Tb) [30], $NaGd(MoO_4)_2$:Eu^{3+},Tb^{3+} [31], $CaMoO_4$:Eu^{3+} [32], $AgRE(WO_4)_2$:Ln^{3+} (RE = Y, La, Gd, Lu; Ln = Eu, Tb, Sm, Dy, Yb/Er, Yb/Tm) [36] and $Gd_2(WO_4)_3$:Tb^{3+}/Eu^{3+} [37] phosphors with excitation wavelength at around 292 nm.

The ET from Tb^{3+} to Eu^{3+} in molybdates has been reported in previous studies [2, 6, 33]. In this paper, a series of experiments were done to demonstrate the ET process between Tb^{3+} and Eu^{3+} in the $NaScMo_2O_8$ host. Figure 4 shows the excitation (a) and emission (b) spectra of the $NaSc_{(0.975-y)}Mo_2O_8$:$0.025Eu^{3+}$, yTb^{3+} ($y = 0$–0.075) sample. The excitation spectra recorded at 618 nm ($^5D_0 \rightarrow {}^7F_2$) of Eu^{3+} are all composed of a broad and strong charge-transfer band of MoO_4^{2-} with peak at 292 nm and a series of typical f–f transitions of Eu^{3+} and Tb^{3+} ions at 395 nm ($^7F_0 \rightarrow {}^5L_6$ of Eu^{3+}), 465 nm ($^7F_0 \rightarrow {}^5D_2$ of Eu^{3+}) and 488 nm ($^7F_6 \rightarrow {}^5D_4$ of Tb^{3+}), except for the excitation intensity (Fig. 4a). The presence of the excitation peak of Tb^{3+} (488 nm, $^7F_6 \rightarrow {}^5D_4$) in the excitation spectrum monitored with Eu^{3+} emission (618 nm, $^5D_0 \rightarrow {}^7F_2$) clearly indicates that an energy transfer has occurred from Tb^{3+} to Eu^{3+} in the $NaScMo_2O_8$ host. As shown in Fig. 4b, under 292 nm excitation (the characteristic peak of MoO_4^{2-}), the emission intensity of Eu^{3+} at 618 nm in $NaSc_{0.965}Mo_2O_8$:$0.025Eu^{3+}$, 0.01 Tb^{3+} (blue line) is much stronger than that of single-doped Eu^{3+} in $NaSc_{0.975}Mo_2O_8$:$0.025Eu^{3+}$ (black line). With increase in Tb^{3+} concentrations, the emission intensity of Eu^{3+} at 618 nm increases gradually and then slowly decreases due to concentration quenching [6]. The emission spectra in Fig. 4b directly support that the ET of $MoO_4^{2-} \rightarrow Tb^{3+} \rightarrow Eu^{3+}$ can take place in the $NaScMo_2O_8$ host. Also taking into account the excitation spectrum in Fig. 4a, if Tb^{3+} ion was excited from $^7F_6 \rightarrow {}^5D_4$ (488 nm), there should be energy transfer from the excited $^5D_4$ level of Tb^{3+} to the $^5D_0$ level of Eu^{3+} in the $NaSc_{(0.975-y)}Mo_2O_8$:$0.025Eu^{3+}$, yTb^{3+} ($y = 0.01$–0.075) samples. Upon excitation into the $^7F_6 \rightarrow {}^5D_4$ transition of Tb^{3+} at 488 nm, the emission spectra of the $NaSc_{0.9}Mo_2O_8$:$0.05Tb^{3+}$, $0.05Eu^{3+}$, $NaSc_{0.95}Mo_2O_8$:$0.05Tb^{3+}$ and $NaSc_{0.95}Mo_2O_8$:$0.05Eu^{3+}$ are presented in Fig. 4c for comparison. The emission

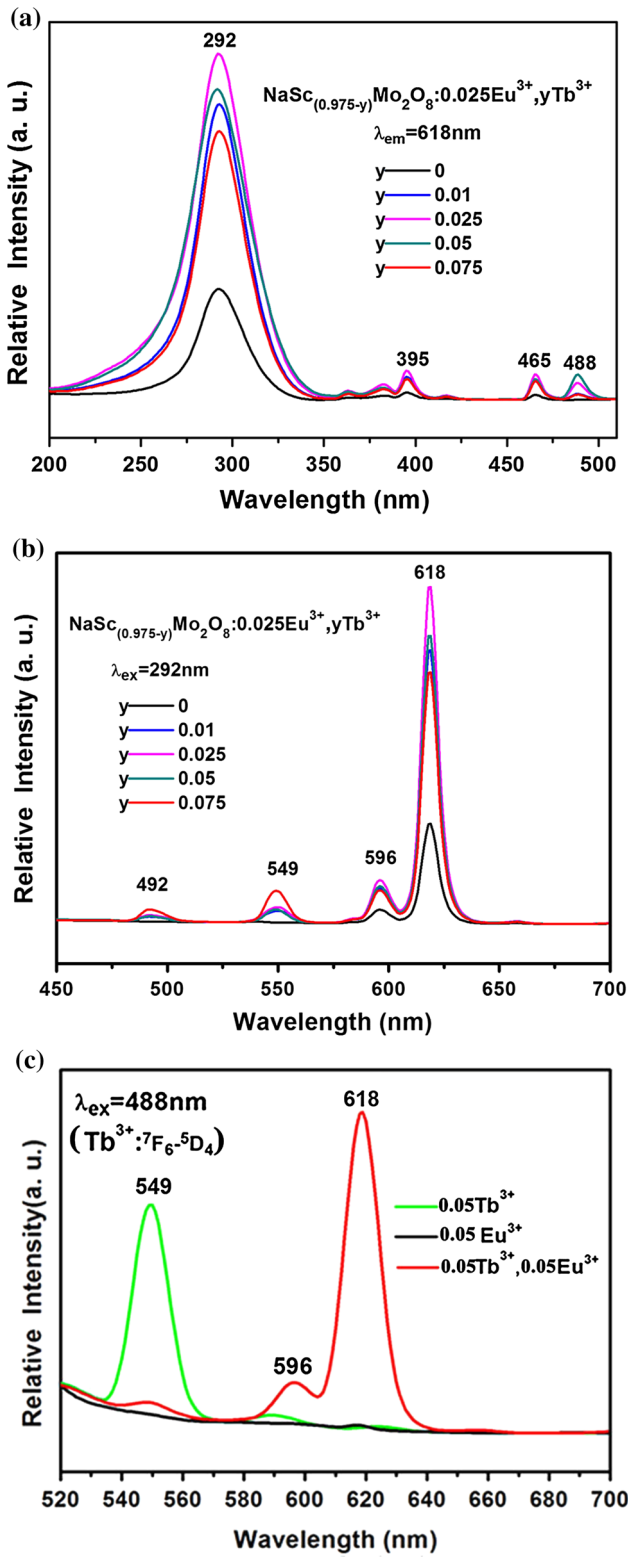

◀**Figure 4** Excitation (**a**) and emission (**b**) spectra of the $NaSc_{0.975}Mo_2O_8$:0.025Eu^{3+}, yTb^{3+} ($y = 0$–0.075) samples. **c** Emission spectra of the $NaSc_{0.9}Mo_2O_8$:0.05Tb^{3+}, 0.05Eu^{3+}, $NaSc_{0.95}Mo_2O_8$:0.05Tb^{3+} and $NaSc_{0.95}Mo_2O_8$:0.05Eu^{3+} samples upon excitation to the $^7F_6 \rightarrow {}^5D_4$ transition of Tb^{3+} at 488 nm, respectively.

spectrum of $NaSc_{0.95}Mo_2O_8$:0.05Tb^{3+} (green line) exhibits the f → f transitions of Tb^{3+} with a strong peak at 549 nm ($^5D_4 \rightarrow {}^7F_5$); there is no obvious emission peak in the $NaSc_{0.95}Mo_2O_8$:0.05Eu^{3+} sample (black one), but the emission spectrum of $NaSc_{0.9}Mo_2O_8$:0.05Tb^{3+}, 0.05Eu^{3+} presents much stronger characteristic peaks of Eu^{3+} at 596 nm ($^5D_0 \rightarrow {}^7F_1$) and 618 nm ($^5D_0 \rightarrow {}^7F_2$) than that of Tb^{3+} at 549 nm ($^5D_4 \rightarrow {}^7F_5$). This phenomenon further demonstrates that the energy can be effectively transferred from Tb^{3+} to Eu^{3+}.

Figure 5a shows the multicolor luminescence based on the ET of $MoO_4^{2-} \rightarrow Tb^{3+} \rightarrow Eu^{3+}$ by changing Eu^{3+} concentration in the $NaSc_{(0.95-x)}Mo_2O_8$:0.05Tb^{3+}, xEu^{3+}. Upon excitation into the MoO_4^{2-} at 292 nm, the $NaSc_{0.95}Mo_2O_8$:0.05Tb^{3+} only emits its characteristic emissions without doping Eu^{3+}; when doped with a small amount of Eu^{3+} ($x = 0.001$), the characteristic emission of Eu^{3+} can be observed apart from Tb^{3+} emission. With increase in Eu^{3+} doping concentrations, the emission intensity of Tb^{3+} at 549 nm ($^5D_4 \rightarrow {}^7F_5$) gradually decreases and that of Eu^{3+} at 618 nm ($^5D_0 \rightarrow {}^7F_2$) and 596 nm ($^5D_0 \rightarrow {}^7F_1$) increases simultaneously because of the energy transfer from Tb^{3+} to Eu^{3+}. And then, the emission spectra of Eu^{3+} gradually become the dominant one with maximum value at $x = 0.1$; with further increasing Eu^{3+}, the emission of Eu^{3+} decreases due to the Eu^{3+}–Eu^{3+} internal concentration quenching effect. The results above further reflect that the energy of the red emission of Eu^{3+} is derived from Tb^{3+} and the multicolor luminescence can be tuned by adjusting the relative ratio of Tb^{3+} to Eu^{3+}. The CIE chromaticity coordinates (Fig. 5b) of $NaSc_{(0.95-x)}Mo_2O_8$:0.05Tb^{3+}, xEu^{3+} vary from green region (0.27, 0.58) to red region (0.62, 0.34) via yellow region (0.42, 0.47) by altering Eu^{3+} concentration, which can be seen clearly from the corresponding

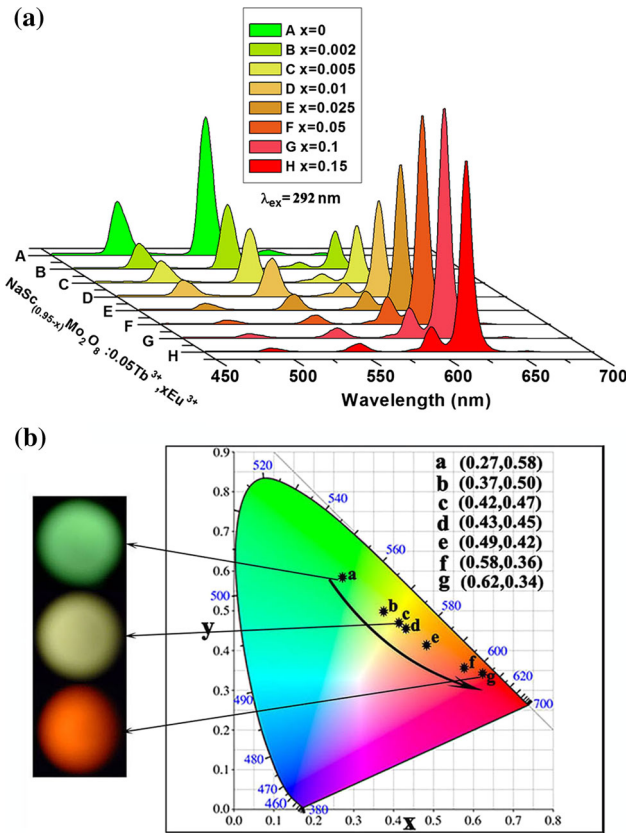

Figure 5 **a** Emission spectra of $NaSc_{(0.95-x)}Mo_2O_8$:0.05Tb^{3+}, xEu^{3+} (x = 0–0.15); **b** the CIE chromaticity coordinates of $NaSc_{(0.95-x)}Mo_2O_8$:0.05Tb^{3+}, xEu^{3+} (x = 0–0.025) phosphors under 292 nm excitation and the corresponding luminescence photographs excited by a 254-nm UV lamp.

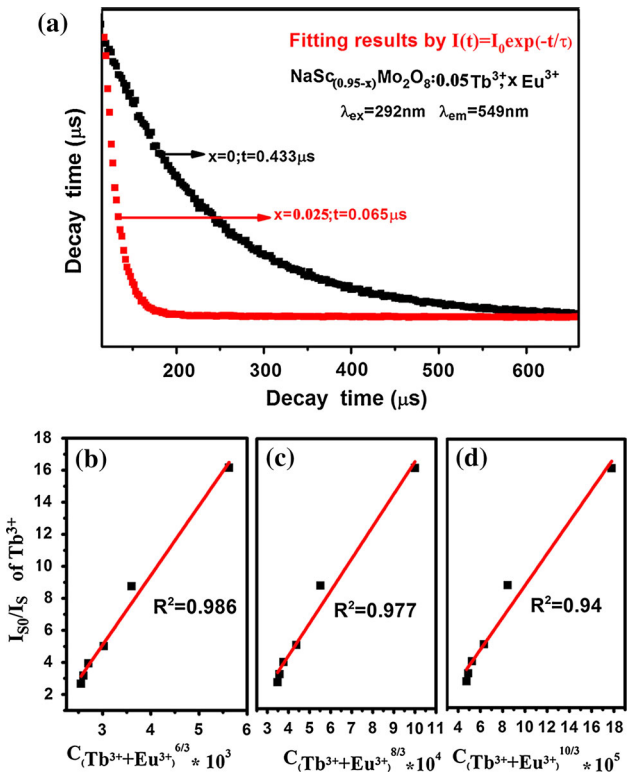

Figure 6 **a** Decay *curves* of Tb^{3+} for the $NaSc_{(0.95-x)}Mo_2O_8$:0.05Tb^{3+}, xEu^{3+} (x = 0 and 0.025) phosphors. **b** The dependence of I_{S0}/I_S of Tb^{3+} on $C_{(Tb^{3+}+Eu^{3+})^{n/3}}$.

luminescence photographs excited by a 254-nm UV lamp (inset in Fig. 5b).

The energy transfer also can be confirmed by the luminescence decay curves of Tb^{3+}, as shown in Fig. 6a. According to Dexter theory [38], the nonradiative energy transfer can shorten the lifetime of Tb^{3+}. The decay time of Tb^{3+} (excited at 292 nm and monitored at 549 nm) as a function of the Eu^{3+} doping concentrations in $NaSc_{(0.95-x)}Mo_2O_8$:0.05Tb^{3+}, xEu^{3+} can be obtained from equation:

$$I_t = I_0 \exp(-t/\tau) \quad (1)$$

where I_t and I_0 are the luminescence intensities at time t and $t = 0$, respectively, and τ is the decay time. The values of Tb^{3+} for $NaSc_{(0.95-x)}Mo_2O_8$:0.05Tb^{3+}, xEu^{3+} are determined to be 0.433 and 0.065 μs at $x = 0$ and 2.5, respectively. We can conclude that with the increase in Eu^{3+} concentration, the fluorescence lifetime of Tb^{3+} ($^5D_4$) state decreases due to the strong energy transfer from Tb^{3+} to Eu^{3+} via nonradiative process in $NaSc_{(0.95-x)}Mo_2O_8$:0.05Tb^{3+}, xEu^{3+} phosphors.

In general, there are two ways for the energy transfer from Tb^{3+} to Eu^{3+} in a phosphor: One is exchange interaction, and the other is electric multipolar interaction. If the critical distance (R_c) between Tb^{3+} and Eu^{3+} is less than 4 Å, the energy transfer takes the exchange interaction; otherwise, it takes the electric multipole interaction. The distance R_c can be calculated using the crystal structure data method through the following equation [39]:

$$R_c = 2\left[\frac{3V}{4\pi X_C N}\right]^{1/3} \quad (2)$$

where N is the number of molecules in the unit cell, V the cell volume and X_c the total concentration of Tb^{3+} and Eu^{3+} ions. For $NaScMo_2O_8$ host ($N = 2$,$V = 370.3$ Å^3), with increasing Eu^{3+} concentration (x = 0.002, 0.025, 0.05 and 0.1) in the $NaSc_{(0.95-x)}Mo_2O_8$:0.05Tb^{3+}, xEu^{3+} sample, the R_c was calculated to be 18.9, 16.8, 15.2 and 13.3 Å at total concentration (X_c) of 0.052, 0.075, 0.10 and 0.15, respectively. All these R_c values are far greater than

4 Å, which indicates that the energy transfer mechanism of $Tb^{3+} \rightarrow Eu^{3+}$ is governed by electric multipolar interaction in $NaScMo_2O_8$ host [40].

The energy transfer mechanism for multipolar interactions can be further discussed by the following equation [41]:

$$\eta_{S0}/\eta_S \propto C^{n/3} \quad (3)$$

Many studies have reported that the value of η_{so}/η_s can be approximately estimated by the luminescence intensity ratio (I_{S0}/I_S) of Tb^{3+} as follows:

$$I_{S0}/I_S \propto C^{n/3} \quad (4)$$

where C is the total concentration of Tb^{3+} and Eu^{3+} and $n = 6$, 8 and 10 are dipole–dipole, dipole–quadrupole and quadrupole–quadrupole interactions, respectively. I_S and I_{S0} are the emission intensity of Tb^{3+} in the presence and absence of Eu^{3+}. The relationships between I_{S0}/I_S and $C_{(Tb^{3+}+Eu^{3+})}{}^{n/3}$ are presented in Fig. 6b. When $n = 6$, the linear behavior fitting value R^2 is 0.986 which is better than others (n = 8, $R^2 = 0.977$ and $n = 10$, $R^2 = 0.94$). The fitting results illustrate that the energy transfer mechanism between Tb^{3+} and Eu^{3+} in $NaScMo_2O_8$ host is dominated by dipole–dipole electric multipolar interaction.

Figure 7 shows detailed schematic for the ET processes of $MoO_4{}^{2-} \rightarrow Tb^{3+} \rightarrow Eu^{3+}$ in $NaScMo_2O_8$ host. Firstly, upon UV irradiation, the energy is absorbed by $MoO_4{}^{2-}$. The electrons in the ground state ($^1A_1$) of $MoO_4{}^{2-}$ shift to its ^1B ($^1T_2$) level [42] and then a very small part of them return to the lowest excited ^1B ($^1T_1$) level to emit the characteristic emission of $MoO_4{}^{2-}$ (Fig. S3 in Supporting Information);

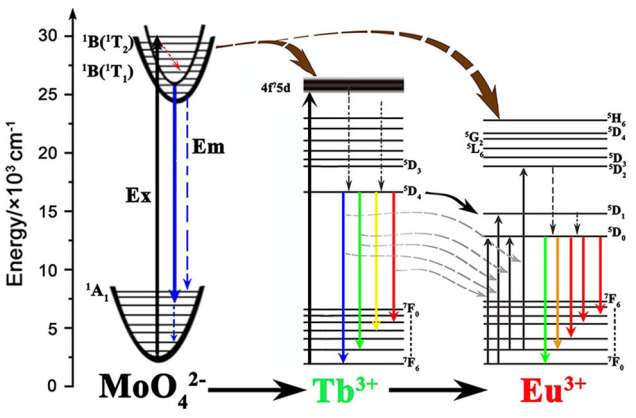

Figure 7 Schematic for the ET processes of $MoO_4{}^{2-} \rightarrow Tb^{3+} \rightarrow Eu^{3+}$ in $NaScMo_2O_8$ host.

meanwhile, other excited electrons transferred energy to Tb^{3+} and Eu^{3+}. On the one hand, the Tb^{3+} ion shows its characteristic emissions: The energy on Tb^{3+} higher levels relaxes to the lowest excited energy level $^5D_4$ via multi-phonon relaxation [40] and then return to the ground state, engendering the emissions of Tb^{3+} ($^5D_4 \rightarrow {}^7F_{6,\ 5,\ 4,\ 3}$). On the other hand, the energy absorbed by Tb^{3+} be transferred to higher excited energy level of Eu^{3+} ($^5D_1$) via dipole–dipole interaction. Finally, the energy on $^5D_1$ level relaxes to $^5D_0$ level, giving out red emissions based on $^5D_0 \rightarrow {}^7F_{0,\ 1,\ 2,\ 3}$ transitions of Eu^{3+}.

Upconversion luminescence

In Fig. 8, under 980 nm excitation, the emission of $NaScMo_2O_8:RE^{3+}$ (RE = Yb/Er, Yb/Ho) showed green (Yb^{3+}/Er^{3+}: $^4S_{3/2}$, $^2H_{11/2} \rightarrow {}^4I_{15/2}$; Yb^{3+}/Ho^{3+}: $^5S_2 \rightarrow {}^5I_8$) luminescence [43]. To gain further insight into the UC emission properties of $NaScMo_2O_8:RE^{3+}$ (RE = Yb/Er, Yb/Ho), the concentration of Er^{3+} (or Ho^{3+}) was fixed at 0.01 and the concentration of the Yb^{3+} was changed from 0 to 0.2 (or from 0 to 0.25). From Fig. 8a, it can be found that the UC emission spectra of $NaSc_{(0.99-x)}Mo_2O_8:xYb^{3+}$, $0.01Er^{3+}$ samples do not show an obvious difference in shape and emission bands except for the emission intensity. All of them exhibit three emission bands centered at 536, 556 and 662 nm, which can be ascribed to the $^2H_{11/2} \rightarrow {}^4I_{15/2}$, $^4S_{3/2} \rightarrow {}^4I_{15/2}$ and $^4F_{9/2} \rightarrow {}^4I_{15/2}$ transitions of Er^{3+}, respectively. Upon variation of the Yb^{3+} concentration from 0 to 0.2, the intensity of UC emission spectra first increases and then decreases. When Yb^{3+} concentration is increased from 0 to 0.1, more Yb^{3+} become available to furnish and transfer energy to the Er^{3+}, resulting in the higher emission intensity. Once exceeded its limit ($x = 0.1$), the interatomic distance between Yb^{3+} and Er^{3+} became short with further increase in the Yb^{3+} concentration, which remarkably enhances the probability of energy migration to the quenching center caused by resonance transfer and then results in the decrease in UC emission intensity. This phenomenon is similar to that of $NaSc_{(0.99-x)}Mo_2O_8:xYb^{3+}$, $0.01Ho^{3+}$, which is given in Fig. 8b. The strong emission band centered at 541 nm, and the relatively weak emission band at 649 nm can be attributed to the $^5S_2 \rightarrow {}^5I_8$ and $^5F_5 \rightarrow {}^5I_8$ transitions of Ho^{3+} ions, respectively. When $x = 0.2$, the sample shows the strongest upconversion luminescence (Fig. 8b).

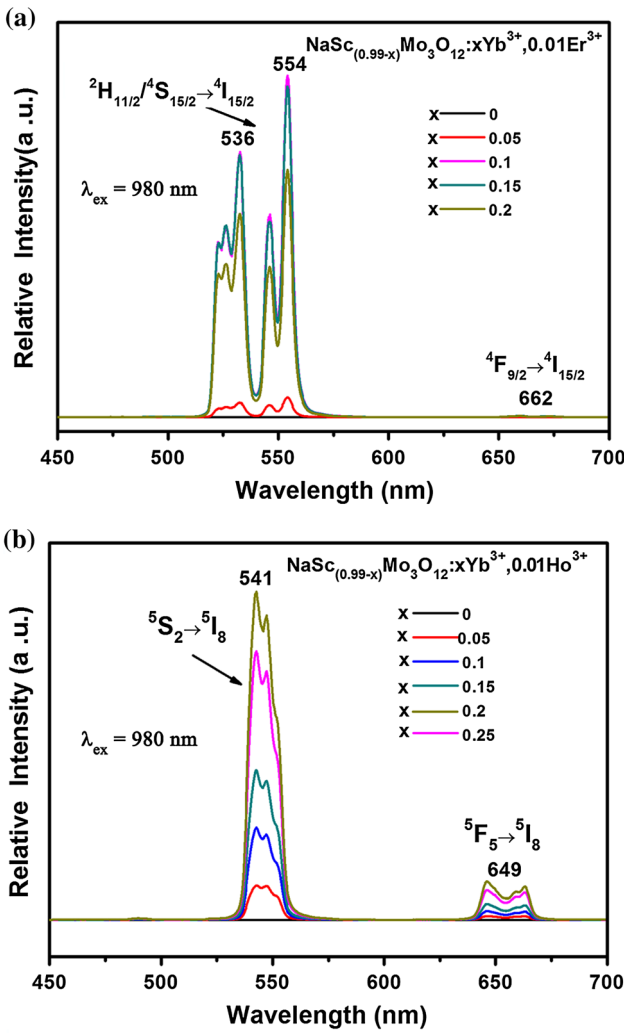

Figure 8 UC emission spectra of **a** the $NaSc_{(0.99-x)}Mo_2O_8$:xYb^{3+}, $0.01Er^{3+}$ (x = 0–0.2) and **b** the $NaSc_{(0.99-x)}Mo_2O_8$:xYb^{3+}, $0.01Ho^{3+}$ (x = 0–0.25) under 980 nm excitation, respectively.

Conclusion

In summary, $NaScMo_2O_8$:RE^{3+} (RE = Tb, Eu, Tb/Eu, Yb/Er, Yb/Ho) phosphors were synthesized by a simple surfactant-free hydrothermal route combined with subsequent calcination at 800 °C. Various ways are enumerated in this paper to prove the ET of $MoO_4^{2-} \rightarrow Tb^{3+} \rightarrow Eu^{3+}$. The $NaSc_{(0.95-x)}Mo_2O_8$:$0.05Tb^{3+}$, xEu^{3+} exhibit strong multicolor emissions from green to red due to the effective ET from Tb^{3+} to Eu^{3+} by dipole–dipole interaction. Upon 980 nm excitation, Yb^{3+}/Er^{3+}- and Yb^{3+}/Ho^{3+}-doped $NaScMo_2O_8$ both exhibit strong green emission. Besides, the Yb^{3+} concentration doped in the $NaSc_{(0.99-x)}Mo_2O_8$:xYb^{3+}, $0.01Er^{3+}$ and $NaSc_{(0.99-x)}Mo_2O_8$:xYb^{3+}, $0.01Ho^{3+}$ phosphors have been optimized at x = 0.1 and 0.2, respectively. Owing to their excellent DC/UC luminescence properties, the $NaScMo_2O_8$:RE^{3+} (RE = Tb, Eu, Tb/Eu, Yb/Er, Yb/Ho) phosphors have great potential application in the fields of color displays and light-emitting devices.

Acknowledgements

This project is financially supported by the National Natural Science Foundation of China (51302229 and 51302228), the Fundamental Research Funds for the Central Universities (XDJK2016C147 and XDJK2015B019) and the Scientific Research Foundation for Returned Scholars, Ministry of Education of China (46th).

Electronic supplementary material: The online version of this article (doi:10.1007/s10853-017-1396-8) contains supplementary material, which is available to authorized users.

References

[1] Wang F, Han Y, Lim CS, Lu YH, Wang JA, Xu J, Chen HY, Zhang C, Hong MH, Liu XJ (2010) Simultaneous phase and size control of upconversion nanocrystals through lanthanide doping. Nature 463:1061–1065

[2] Li Y, Wang GF, Pan K, Zhou W, Wang C, Fan NY, Chen YJ, Feng QM, Zhao BB (2012) Controlled synthesis and luminescence properties of rhombic $NaLn(MoO_4)_2$ submicrocrystals. CrystEngComm 14:5015–5020

[3] Riwotzki K, Meyssamy H, Schnablegger H, Kornowski A, Haase M (2001) Liquid-phase synthesis of colloids and redispersible powders of strongly luminescing LaPO4:Ce, Tb nanocrystals. Angew Chem Int Ed 40:573–576

[4] Wang GF, Qin WP, Zhang JS, Zhang JS, Wang Y, Cao CY, Wang LL, Wei GD, Zhu PF, Kim RJ (2008) Synthesis, growth mechanism, and tunable upconversion luminescence of Yb^{3+}/Tm^{3+}-codoped YF_3 nanobundles. J Phys Chem C 112:12161–12167

[5] Huang J, Xu J, Luo H, Xu X, Li Y (2011) Effect of alkali-metal ions on the local structure and luminescence for double tungstate compounds $AEu(WO_4)_2$ (A = Li, Na, K). Inorg Chem 50:11487–11492

[6] Zhao B, Yuan L, Hu SS, Zhang XM, Zhou XJ, Tang JF, Yang J (2016) One-step hydrothermal synthesis of $Sc_2Mo_3O_{12}$:Ln^{3+} (Ln = Eu, Tb, Dy, Tb/Eu, Dy/Eu) nanosheets and

their multicolor tunable luminescence. New J Chem 40:9211–9222

[7] Hou L, Cui SB, Fu ZL, Wu ZJ, Fu XH, Jeong JH (2014) Facile template free synthesis of KLa(MoO4)2:Eu^{3+}, Tb^{3+} microspheres and their multicolor tunable luminescence. Dalton Trans 43:5382–5392

[8] Cui SB, Zhu YS, Xu W, Zhou PW, Xia L, Chen X, Song HW, Han W (2014) Self-assembly and modified luminescence properties of $NaY(MoO_4)_2$:Tb^{3+}, Eu^{3+} inverse opals. Dalton Trans 43:13293–13298

[9] Zheng H, Chen BJ, Yu HQ, Sun JS, Lia XP, Zhang JS, Zhong H, Wu ZL, Xia HP (2015) Influence of microwave hydrothermal reaction factor on the morphology of $NaY(MoO_4)_2$ nano-/micro-structures and luminescence properties of $NaY(MoO_4)_2$:Tb^{3+}. RSC Adv 5:56337–56347

[10] Xu L, Yang XY, Zhai Z, Chao X, Zhang ZH, Hou WH (2011) EDTA-mediated hydrothermal synthesis of $NaEu(MoO_4)_2$ microrugbies with tunable size and enhanced luminescence properties. CrystEngComm 13:4921–4929

[11] Yang XX, Fu ZL, Liu GF, Zhang CP, Wei YL, Wu ZJ, Sheng TQ (2015) Controlled morphology and EDTA-induced pure green upconversion luminescence of Er^{3+}/Ho^{3+}–Yb^{3+} co-doped $NaCe(MoO_4)_2$ phosphor. RSC Adv 5:70220–70228

[12] Xu ZH, Li CX, Li GG, Chai RT, Peng C, Yang DM, Lin J (2010) Self-assembled 3D urchin-like $NaY(MoO_4)_2$:Eu^{3+}/Tb^{3+} microarchitectures: hydrothermal synthesis and tunable emission colors. J Phys Chem C 114:2573–2582

[13] Katelnikovas A, Plewa JL, Sakirzanovas S, Dutczak D, Enseling D, Baur F, Winkler H, Kareiv A, Jüstel T (2012) Synthesis and optical properties of $Li_3Ba_2La_3(MoO_4)_8$:Eu^{3+} powders and ceramics for pcLEDs. J Mater Chem 22:22126–22134

[14] Zhou J, Xia ZG (2014) Multi-color emission evolution and energy transfer behavior of $La_3GaGe_5O_{16}$:Tb^{3+}, Eu^{3+} phosphors. J Mater Chem C 2:6978–6984

[15] Wang Y, Brik MG, Dorenbos P, Huang Y, Tao Y, Liang H (2014) Enhanced green emission of Eu^{2+} by energy transfer from the $^5D_3$ level of Tb^{3+} in $NaCaPO_4$. J Phys Chem C 118:7002–7009

[16] Zhang Y, Geng D, Kang X, Shang M, Wu Y, Li X, Lian H, Cheng Z, Lin J (2013) Rapid, large-scale, morphology-controllable synthesis of YOF:Ln^{3+} (Ln = Tb, Eu, Tm, Dy, Ho, Sm) nano-/microstructures with multicolor-tunable emission properties. Inorg Chem 52:12986–12994

[17] Atabaev TS, Lee JH, Han DW, Hwang YH, Kim HK (2012) Cytotoxicity and cell imaging potentials of submicron color-tunable yttria particles. J Biomed Mater Res A 100:2287–2294

[18] Wen DW, Feng JJ, Li JH, Shi JX, Wu MM, Su Q (2015) K2Ln(PO4)(WO4):Tb^{3+}, Eu^{3+} (Ln = Y, Gd and Lu) phosphors: highly efficient pure red and tuneable emission for white light-emitting diodes. J Mater Chem C 3:2107–2114

[19] Guo N, Song Y, You H, Jia G, Yang M, Liu K, Zheng Y, Huang Y, Zhang H (2010) Optical properties and energy transfer of $NaCaPO_4$:Ce^{3+}, Tb^{3+} phosphors for potential application in light-emitting diodes. Eur J Inorg Chem 29:4636–4642

[20] You H, Wu X, Hong G, Tang J, Hu H (2003) A new type of highly efficient luminescent material the system Al_2O_3–B_2O_3 containing Ce^{3+} and Tb^{3+} ions. Chem Mater 15:2000–2004

[21] Wang D, Wang Y, He JW (2012) Investigation of energy absorption and transfer process of Tb^{3+} or Eu^{3+} excited $Na_3Gd(PO_4)_2$ in the VUV region. Mater Res Bull 47:142–145

[22] Pavani K, Suresh Kumar J, Rama Moorthy L (2014) Photoluminescence properties of Tb^{3+} and Eu^{3+} ions co-doped $SrMg_2La_2W_2O_{12}$ phosphors for solid state lighting applications. J Alloys Compd 586:722–799

[23] Geng DQ, Li GG, Shang MM, Peng C, Zhang Y, Cheng ZY, Lin J (2012) Nanocrystalline $CaYAlO_4$:Tb^{3+}/Eu^{3+} as promising phosphors for full-color field emission displays. Dalton Trans 41:3078–3086

[24] Zhu Y, Xu W, Cui S (2015) Controlled size and morphology, and phase transition of YF3:Yb^{3+}, Er^{3+} and YOF:Yb^{3+}, Er^{3+} nanocrystals for fine color tuning. J Mater Chem C 4:331–339

[25] Zhang C, Zhou HP, Liao LY, Feng W, Sun W, Li ZX, Xu CH, Fang CJ, Sun LD, Zhang YW, Yan CH (2010) Luminescence modulation of ordered upconversion nanopatterns by a photochromic diarylethene: rewritable optical storage with nondestructive readout. Adv Mater 22:633–637

[26] Pichaandi J, Boyer JC, Delaney KR (2011) Two-photon upconversion laser (scanning and wide-field) microscopy using Ln^{3+}-doped $NaYF_4$ upconverting nanocrystals: a critical evaluation of their performance and potential in bioimaging. J Phys Chem C 115:19054–19064

[27] Li CX, Yang DM, Ma PA, Chen YY, Wu Y, Hou ZY, Dai YL, Zhao JH, Sui CP, Lin J (2013) Multifunctional upconversion mesoporous silica nanostructures for dual modal imaging and in vivo drug delivery. Small 9:4150–4159

[28] Liao J, Nie L, Wang Q (2016) $NaGd(WO_4)_2$:Yb^{3+}/Er^{3+} phosphors: hydrothermal synthesis, optical spectroscopy and green upconverted temperature sensing behavior. RSC Adv 6:35152–35159

[29] Wang Z, Feng J, Pang M, Pan SH, Zhang HJ (2013) Multicolor and bright white upconversion luminescence from rice-shaped lanthanide doped BiPO4 submicron particles. Dalton Trans 42:12101–12108

[30] Wang DM, Fan J, Shang MM, Li K, Zhang Y, Lian HZ, Lin J (2016) Pechini-type sol–gel synthesis and multicolor-tunable emission properties of $GdY(MoO_4)_3:RE^{3+}$ (RE = Eu, Dy, Sm, Tb) phosphors. Opt Mater 51:162–170

[31] Li AM, Xu DK, Lin H, Yang SH, Shao YZ, Zhang YL, Chen ZQ (2015) Facile morphology-controllable hydrothermal synthesis and color tunable luminescence properties of NaGd(MoO4)2:Eu^{3+}, Tb^{3+} microcrystals. RSC Adv 5:45693–45702

[32] Rama Raju GS, Pavitra E, Ko YH, Yu JS (2012) A facile and efficient strategy for the preparation of stable $CaMoO_4$ spherulites using ammonium molybdate as a molybdenum source and their excitation induced tunable luminescent properties for optical applications. J Mater Chem 22:15562–15569

[33] Fu ZL, Xia WW, Li QS (2012) Highly uniform $NaLa(MoO_4)_2:Ln^{3+}$(Ln = Eu, Dy) microspheres: template-free hydrothermal synthesis, growing mechanism, and luminescent properties. CrystEngComm 14:4618–4624

[34] Zhao B, Yuan L, Hu SS, Zhang XM, Zhou XJ, Tang JF, Yang J (2016) Controllable synthesis of $Sc_2Mo_3O_{12}$ microcrystals with exposed 001 facets and their remarkable tunable luminescence properties by doping lanthanides. CrystEngComm 18:8044–8058

[35] Tian Y, Qi XH, Wu XW, Hua RN, Chen BJ (2009) Luminescent properties of Y_2 $(MoO_4)_3:Eu^{3+}$ red phosphors with flowerlike shape prepared via coprecipitation method. J Phys Chem C 113:10767–10772

[36] Zhou Y, Yan B, He XH (2014) Controlled synthesis and up/down-conversion luminescence of self-assembled hierarchical architectures of monoclinic $AgRE(WO_4)_2:Ln^{3+}$ (RE = Y, La, Gd, Lu; Ln = Eu, Tb, Sm, Dy, Yb/Er, Yb/Tm). J Mater Chem C 2:848–855

[37] Zeng YB, Li ZQ, Wang LM, Xiong YJ (2012) Controlled synthesis of $Gd_2(WO_4)_3$ microstructures and their tunable photoluminescent properties after Eu^{3+}/Tb^{3+} doping. CrystEngComm 14:7043–7048

[38] Blasse G (1969) Energy transfer in oxidic phosphors. Philips Res Rep 24:131–144

[39] Zhang Y, Gong WT, Yu JJ, Lin Y, Ning GL (2015) Tunable white-light emission via energy transfer in single-phase $LiGd(WO_4)_2:Re^{3+}$ (Re = Tm, Tb, Dy, Eu) phosphors for UV-excited WLEDs. RSC Adv 5:96272–96280

[40] Zhang XG, Zhou LY, Pang Q, Shi JX, Gong ML (2014) Tunable luminescence and $Ce^{3+} \rightarrow Tb^{3+} \rightarrow Eu^{3+}$ energy transfer of broadband-excited and narrow line red emitting Y2SiO5:Ce^{3+}, Tb^{3+}, Eu^{3+} phosphor. J Phys Chem C 118:7591–7598

[41] Zhou J, Xia ZG (2015) Luminescence color tuning of Ce^{3+}, Tb^{3+} and Eu^{3+} codoped and tri-doped $BaY_2Si_3O_{10}$ phosphors via energy transfer. J Mater Chem C 3:7552–7560

[42] Zhang Y, Holzwarth NAW, Williams RT (1998) Electronic band structures of the scheelite materials $CaMoO_4$, $CaWO_4$, $PbMoO_4$, and $PbWO_4$. Phys Rev B 57:12738–12750

[43] Huang SH, Zhang X, Wang LZ, Bai L, Xu J, Li CX, Yang PP (2012) Controllable synthesis and tunable luminescence properties of $Y_2(WO_4)_3:Ln^{3+}$ (Ln = Eu, Yb/Er, Yb/Tm and Yb/Ho) 3D hierarchical architectures. Dalton Trans 41:5634–5642